Fluctuations, Order, and Disorder in Short Diblock Copolymers

Sangwoo Lee, Timothy M. Gillard, and Frank S. Bates
Dept. of Chemical Engineering and Materials Science, 421 Washington Avenue SE, University of Minnesota, Minneapolis, MN 55455

DOI 10.1002/aic.14023
Published online February 11, 2013 in Wiley Online Library (wileyonlinelibrary.com)

The phase behavior for a series of poly(1,4-isoprene-b-DL-lactide) diblock copolymers characterized by a relatively large Flory–Huggins segment–segment interaction parameter (χ) and low degrees of polymerization (N) over a range of compositions was reported. Ordered-state morphologies were deduced from small-angle x-ray scattering (SAXS) measurements, and $\chi(T)$ was determined from order-disorder transition temperatures (T_{ODT}'s) associated with the compositionally symmetric specimens and assuming the mean-field theory, that is, $(\chi N)_{ODT}=10.5$. The ODT was determined by differential scanning calorimetry, SAXS, and dynamic mechanical spectroscopy, and shown to be weakly first-order, with latent heats of transition that vary strongly with composition. We interpret this behavior in terms of the mean and Gauss interfacial curvature of the ordered-state morphologies and with respect to composition fluctuations in the disordered state. These results offer a fresh strategy for investigating weakly first-order phase transitions within the Brazovskii universality class. © 2013 American Institute of Chemical Engineers *AIChE J*, 59: 3502–3513, 2013
Keywords: block copolymers, fluctuations, phase behavior

Introduction

In 1970, Neal Amundson was pressured by the administration at the University of Minnesota to absorb a group of metallurgists into the Department of Chemical Engineering after disbanding the program in Mining and Metallurgy. Amundson resisted this move, fortunately unsuccessfully, acquiescing only after securing a dowry: new faculty for expansion into the growing field of polymer science and engineering. Today, materials science and engineering represents a key strength of the department, and the polymer program has grown to embrace more than a half-dozen faculty across Chemical Engineering and Materials Science, and Chemistry, currently supporting more than 100 Ph.D. candidates and postdoctoral fellows. A central theme is multiblock polymers, a field with a bright future[1] due in part to Amundson's boundless legacy. This article on the fundamental thermodynamics of simple diblock copolymers is a tribute to the Chief.

Block polymers have fascinated researchers for decades, combining a host of interesting scientific questions with commercial relevance.[2–4] Many new and exciting applications require ever decreasing nanoscale dimensions (e.g., lithographic patterning of microelectronic materials),[5] which has drawn us into exploring the thermodynamic behavior of block copolymers (BCP's) characterized by large Flory-Huggins segment–segment interaction parameters (χ's). Because the state of segregation of a BCP depends on the compound variable χN, where N is the overall degree of polymerization, large values of χ produce ordered nanostructures (often referred to as microphase separation) even at relatively low values of N.[6] Our interest in such high χ, low N materials is two-fold. First, as a practical matter we wish to understand the lower limit of the range of characteristic dimensions, and the associated physical properties, which can be accessed using BCPs. However, mean-field treatments of BCP phase behavior are typically formulated in the limit of infinitely large N, that is, infinitesimally small χ. As N is reduced from this limit composition fluctuations are expected to become increasingly important. A second objective is to expand our fundamental understanding of the thermodynamic behavior of this class of materials under circumstances where the assumptions inherent in the accepted theoretical framework used to describe BCP self-assembly[6,7] would be expected to fail.

In the mean-field limit, Leibler predicted that AB diblock copolymer phase behavior depends on two parameters: the volume fraction f of block A and the combined parameter χN.[3,6,8–11] The composition, f, which is determined by the degree of polymerization of each block (and to a lesser extent the repeat unit densities), primarily controls the geometry of the ordered microphase separated structures, whereas χN dictates the strength of segregation between the blocks. For systems governed by van der Waals interactions, χ is proportional to the inverse of temperature: $\chi=\alpha/T+\beta$ where α and β are empirically determined constants and T is the temperature. The magnitude of χ is determined by the chemical structure of the repeat units, which can be approximated (in the absence of specific interactions such as hydrogen bonding) based on the associated solubility parameters (δ_i): $\chi=(V/RT)(\delta_A-\delta_B)^2$ where V is the repeat unit molar volume and R is the gas constant. Thus, heating a BCP melt generally reduces χN. Leibler showed that within mean-field

S. Lee and T. M. Gillard contributed equally to this work.
Correspondence concerning this article should be addressed to F. S. Bates at bates001@umn.edu.

theory the phase transition from a state of disorder to order, known as the order-disorder transition (ODT), occurs at a critical point: $(\chi N)_{ODT}=10.5$ for symmetric ($f=1/2$) BCPs. At this continuous, second-order, phase transition, the homogeneous disordered state gives way to an ordered lamellar phase with a composition profile of differential amplitude. This amplitude then grows as χN is increased, for example, by decreasing the temperature.

Following a seminal publication by Brazovskii,[12] Frederickson and Helfand proposed a correction to Leibler's theory to account for the effects of fluctuations at finite N.[7] In this theory, the disordered state in the vicinity of the ODT is no longer homogeneous, but is instead characterized by thermally induced local composition fluctuations with a characteristic length scale on the order of the radius of gyration of the polymer chain. The amplitude of these fluctuations increases as χN is raised, producing a degree of disordered microphase segregation at values of χN well-below the transition to the ordered phase. These fluctuations stabilize the disordered phase and shift the value of $(\chi N)_{ODT}$ to a value greater than 10.5, the magnitude of which increases with decreasing N. Composition fluctuations break the second-order character of the ODT for symmetric diblocks resulting in a discontinuous, fluctuation-induced weakly first-order phase transition. The theory predicts a small discontinuous change in the local composition profile at the ODT coincident with the fluctuating disordered state transforming to the ordered lamellar morphology. Although only strictly valid at values of N approaching 10^9 and not considered quantitatively accurate, the Fredrickson–Helfand theory has been remarkably successful at capturing certain qualitative features of the phase behavior of real BCP materials including the topology of the diblock copolymer phase diagram and the presence of fluctuations near the ODT. In this work, we explore the ODT and phase behavior of BCP materials characterized by unusually small molecular weights, $N<100$, which is well-outside the limits where the fluctuation theory is expected to be applicable.

With a few notable exceptions,[13–19] the thermodynamics associated with the ODT in general, and the effects of fluctuations specifically, have been studied using indirect experimental techniques, for example, rheology and small-angle scattering.[20,21] In this report, we present experimental results obtained with a series of high χ, low N poly(1,4-isoprene-*b*-DL-lactide) (IL) diblock copolymers in which direct calorimetric measurement of the ODT was possible. This system was chosen based on the large difference in solubility parameters between poly(isoprene) (PI; $\delta_{PI}=16.6$ J$^{1/2}$/cm$^{3/2}$) and poly(DL-lactide) (PLA; $\delta_{PLA}=19.7$ J$^{1/2}$/cm$^{3/2}$).[22,23] The thermodynamic properties near the ODT were systematically explored using a combination of small-angle x-ray scattering (SAXS), dynamic mechanical spectroscopy (DMS), and differential scanning calorimetry (DSC) experiments, including direct thermal measurements of the ODT for samples that span the primary diblock copolymer morphologies, including ordered lamellae, cylinders, and spheres. $\chi(T)$ was estimated, and the phase behavior for this system was characterized near the order to disorder transition phase boundary and mapped on a phase portrait.

Experimental

Materials and molecular characterizations

A detailed synthetic scheme for the preparation of IL diblock copolymers is described elsewhere.[24] Briefly, ω-hydroxyl poly(1,4-isoprene) (PI-OH) was prepared by anionic polymerization of isoprene and used as a macroinitiator for the ring-opening polymerization of lactide monomer using a triethyl aluminum catalyst yielding poly(1,4-isoprene-*b*-DL-lactide) (IL). The molecular weights and block compositions of IL polymers were determined by ^{1}H nuclear magnetic resonance spectroscopy experiments (Varian VI-500), and dispersities ($Đ=M_w/M_n$) were determined by size exclusion chromatography (SEC) using chloroform as the mobile phase.

Dynamic mechanical spectroscopy

Order-disorder and order-order transition temperatures (T_{ODT} and T_{OOT}, respectively) of each IL diblock copolymer were measured using DMS experiments conducted with a Rheometrics ARES strain controlled mechanical spectrometer.[21] The IL diblock copolymers were loaded between 25 mm parallel plates, disordered by heating above the T_{ODT}, cooled, and heated at a rate of 0.1°C/min while measuring the isochronal ($\omega=0.1$ rad/s) linear dynamic shear storage (G') and loss (G'') moduli. The T_{ODT}s were obtained from the final heating step and were taken as the temperature at which G' shows a precipitous drop to a liquid-like response. T_{OOT}'s were associated with rapid changes in G' that separated nonterminal (soft solid) viscoelastic states.

Differential scanning calorimetry

A TA Instrument Q1000 DSC was used to measure the glass transition temperatures (T_g) of the PI and PLA blocks. Samples (~10 mg) were placed in hermetically sealed aluminum pans, heated to 200°C, cooled to −100°C, and heated to 200°C again at a rate of 10°C/min. The T_g values were determined using the final heating results.

Many DSC thermograms of the IL diblock copolymers showed distinct thermal features on cooling and heating with onset temperatures corresponding with the T_{ODT}'s of the materials. This phenomenon was further examined in selected IL diblock copolymers using a TA Instruments Discovery DSC. In these experiments, samples (10–20 mg) in aluminum Tzero hermetic DSC pans were equilibrated at a temperature 50–75°C above the T_{ODT}, cooled at a specified rate through the ODT to 0°C (−20°C in the case of IL-15), and then heated through the ODT to the initial equilibration temperature. For selected samples, an annealing step at a temperature approximately 20°C below T_{ODT} was employed between the initial cooling and the final heating steps. The latent enthalpy of the ODT phase transition, ΔH_{ODT}, was determined from the DSC thermograms using TA Instruments Trios software. Thermal degradation was not observed by SEC analysis of the samples after DSC experiments.

Small angle x-ray scattering

The phase behavior of the IL diblock copolymers was investigated using SAXS experiments conducted at DND-CAT (beamline 5-ID-D) at the Advanced Photon Source located at Argonne National Laboratory (Argonne, IL). The sample-to-detector distances employed for the experiments were 3.97, 4.03, 4.63, or 5.5 m, and the x-ray wavelength, λ, was 0.729 Å. Scattering data were collected with a Mar area CCD detector, and azimuthally integrated to the one-dimensional (1-D) form of intensity, I, vs. scattering momentum transfer vector, $q=4\pi\lambda^{-1}\sin(\theta/2)$, where θ is the scattering angle. For isothermal experiments, the samples were placed

Table 1. Molecular Characterization Data for IL Diblock Copolymers

Polymer	$M_{n,I}$* (g/mol)	$M_{n,L}$* (g/mol)	M_n* (g/mol)	f_L†	$Đ$	N‡	$T_{g,\ PLA}$ (°C)
I-1	1130	–		–	1.06	19	–
I-2	1350	–		–	1.06	23	–
I-3	1720	–		–	1.07	29	–
I-4	2810	–		–	1.06	47	–
I-5	3880	–		–	1.07	57	–
IL-1	1130	1620	2750	0.51	1.12	39	20
IL-2	1350	2200	3550	0.54	1.09	49	22
IL-3	1720	2810	4530	0.54	1.09	63	29
IL-5	1130	4260	5390	0.73	1.08	71	29
IL-6	1130	3140	4270	0.67	1.08	57	28
IL-7	1350	2340	3690	0.56	1.11	51	21
IL-8	1350	3030	4380	0.62	1.13	59	35
IL-9	1130	4930	6060	0.76	1.08	79	35
IL-10	1720	2360	4080	0.50	1.11	57	24
IL-11	1720	1620	3340	0.40	1.10	48	11
IL-12	2810	1190	4000	0.23	1.11	62	5
IL-13	2810	1320	4130	0.25	1.13	63	11
IL-14	2810	1770	4580	0.31	1.15	69	15
IL-15	2810	1080	3890	0.22	1.12	60	5
IL-16	2810	2220	5030	0.36	1.04	74	32
IL-24	3880	1090	4970	0.17	1.08	79	4

*Number average molecular weight.
†Calculated volume fraction of PLA using bulk densities of PI (0.9 g/cm^3) and PLA (1.25 g/cm^3) at 25°C with experimental error ±0.01.[22,25]
‡Number average degree of polymerization with the reference volume of $V_{ref}=(V_{PI}V_{PLA})^{1/2}\approx 110$ Å^3 where V_{PI} and V_{PLA} are PI and PLA unit segment volumes at room temperature, respectively.

in aluminum DSC pans and the temperature was controlled using a Linkam DSC stage cooled with liquid nitrogen and maintained under an inert (helium or nitrogen) atmosphere. The samples were first heated above the T_{ODT} then cooled to various target temperatures and held for 2 min before data collection, unless otherwise specified. Temperature changes were implemented at a rate of approximately 100°C/min.

Dynamic temperature ramp SAXS experiments were also conducted on select samples to mimic the DSC measurements used to evaluate the ODT. In these experiments, samples were placed in 1.5-mm diameter quartz capillaries, and the temperature was controlled using a modified Linkam HFS91 hot stage. The samples were equilibrated at a temperature above the T_{ODT} (150, 160, and 100°C for IL-1, IL-14, and IL-15 samples, respectively), cooled at a controlled ramp rate to a temperature well-below T_{ODT} (30, 40, and 0°C for IL-1, IL-14, and IL-15, respectively), held at the lowest temperature for 2–10 min, and finally heated at a controlled ramp rate to the original equilibration temperature above the T_{ODT}. Scattering patterns were collected *in situ* in intervals of 10°C while the temperature was ramped. Analogous experiments were conducted over a narrower temperature range in the vicinity of the T_{ODT} (85–100°C, and 120–140°C for IL-1 and IL-14, respectively) with scattering patterns collected every 1°C. The scattering invariant, Q_{rel}, was calculated by numerically integrating the intensity data (see Eq. 4) over the range of q that was experimentally accessible (~0.02–0.26 Å^{-1}) after subtracting a background intensity obtained from an empty capillary. The principle scattering peak of the 1-D SAXS patterns were fit to Lorentzian (ordered states) or quadratic (disordered state) functions for precise extraction of q* values.

Results

A series of 16 IL diblock copolymers was synthesized from five PI-OH precursors with a wide range of PLA block volume fractions, $0.17\leq f_L\leq 0.76$ (Table 1). The T_{ODT}'s of these samples, obtained from DMS and DSC experiments, fall within an experimentally feasible temperature window (< 200°C) except IL-16 (see below). The ODTs were confirmed and ordered morphologies identified with isothermal synchrotron SAXS experiments. Five characteristic SAXS patterns provide definitive phase assignments as listed in Table 2 (representative examples shown in Figure 1): disorder—DIS, the Frank–Kasper sigma phase—σ (IL-15), body-centered cubic spheres—BCC (IL-15 and 24), hexagonally packed cylinders—HEX (IL-5, 9, 12, 13, 14, and 16), and lamellae—LAM (IL-1, 2, 3, 6, 7, 8, and 10).

In addition to the typical rheological method used to identify the T_{ODT} (taken as the temperature at which a

Table 2. Phase Behavior of IL Diblock Copolymers

Polymer	Phase and Phase Transition Temperature (°C)§	q* (1/Å) (Sample Temperature in °C, Phase)†
IL-1‡	LAM—93(96)—DIS	0.0736 (50, LAM)
IL-2‡	LAM—110(114)—DIS	0.0699 (50, LAM)
IL-3‡	LAM—153(157)—DIS	0.0604 (50, LAM)
IL-5	HEX—95(98)—DIS	0.0676 (90, HEX)
IL-6	LAM—77—DIS	0.0658 (50, LAM)
IL-7‡	LAM—111(112)—DIS	0.0685 (50, LAM)
IL-8	LAM—110—DIS	0.0615 (50, LAM)
IL-9	HEX—97—DIS	0.0590 (25, HEX)
IL-10‡	LAM—146(147)—DIS	0.0628 (50, LAM)
IL-11	LAM—98—DIS	0.0697 (50, LAM)
IL-12	HEX—65—DIS	0.0674 (50, HEX)
IL-13	HEX—105(105)—DIS	0.0605 (25, HEX)
IL-14	HEX—130(132)—DIS	0.0595 (57, HEX)
IL-15	σ-Phase—27—BCC—50(51)—DIS	0.0648 (40, BCC)
IL-16	HEX—200<DIS	0.0392 (200, HEX)
IL-24	BCC—76—DIS	0.0664 (45, BCC)

§$T_{ODT,}$ and T_{OOT} were measured by DMS. Values listed in parenthesis were determined by DSC.
†Principal peak positions (q*) determined by SAXS patterns at the temperature and phase indicated in the parenthesis.
‡Polymers used for determining χ_{IL}.

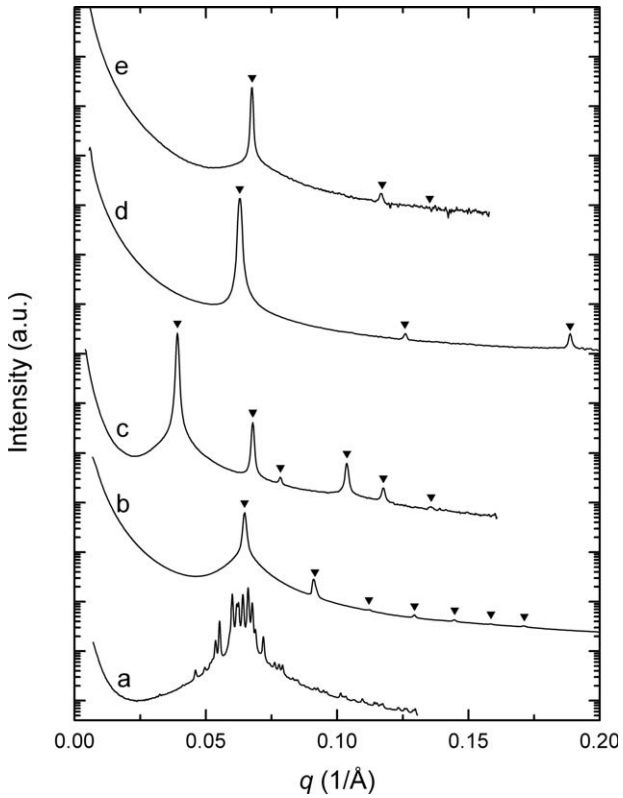

Figure 1. SAXS with varying composition.

Isothermal synchrotron SAXS patterns obtained from the IL diblock copolymers. (a) σ-phase identified with IL-15 (f_L=0.22) after 26 days aging at room temperature. (b) BCC phase identified with IL-15 (f_L=0.22) after 30 min annealing at 40°C. The relative peak positions of BCC phase, q/q^* = √1, √2, √3, √4, √5, √6, √7 are marked by inverse triangles where q^* is the primary peak. (c) HEX phase identified with IL-16 (f_L=0.36) at 200°C with q/q^* = √1, √3, √4, √7, √9, √12. (d) LAM phase identified with IL-10 (f_L=0.50) at 50°C with q/q^* = √1, √4, √9 (e) HEX phase identified with IL-5 (f_L=0.73) at 90°C with q/q^* = √1, √3, √4.

precipitous drop in G' is observed on slow heating from the ordered state), many IL diblock copolymer samples showed a weak but distinct thermal signature of the ODT in DSC experiments. The details of this thermal signature were found to be strongly dependent on the ordered-phase morphology. Representative DMS and DSC data used to identify T_{ODT}s for IL copolymers that form LAM, HEX, and ordered spheres (BCC and/or σ) are shown in Figure 2. Peaks are visible in the DSC thermograms with onset temperatures that coincide closely with the rheological signatures of the ODT. We attribute these endothermic peaks to the latent heat associated with the ODT, and take the onset of this temperature response as the T_{ODT}. We accepted the T_{ODT}s obtained from DMS measurements as the equilibrium values due to the much slower heating rate and more quantitative signatures compared to the DSC measurements. A detailed analysis of the DSC results is presented below.

We have estimated $\chi_{IL}(T)$ using the T_{ODT}s determined for the symmetric and nearly symmetric ($f_L \approx 0.5$) IL polymers (IL-1, 2, 3, 7, and 10) based on mean-field theory, assuming $(\chi N)_{ODT}$=10.5.[6] The degree of polymerization N was determined using a segment reference volume, v=110 Å^3, approximately the geometric average for PI and PLA. A linear function of the form $\chi_{IL}=\alpha/T+\beta$ was extracted from the T_{ODT}s and the result is plotted in Figure 3, yielding

$$\chi_{IL}^{110}=\frac{(230\pm60)}{T}-(0.38\pm0.14) \quad (1)$$

DSC thermograms obtained on cooling and heating at various temperature ramp rates from representative LAM (IL-1), HEX (IL-14), and BCC (IL-15) forming IL samples are shown in Figure 4. The qualitative and quantitative features of the thermal response at the ODT are strongly dependent on the ordered-phase morphology. Although the thermal signature of the ODT was weak for all samples, the LAM samples exhibited the strongest features comparatively. For LAM samples, peaks we attribute to the ODT were clearly visible for the disorder-to-order transition on cooling and the order-to-disorder transition on heating at all temperature ramp rates tested, as shown for IL-1 in Figure 4A. HEX samples also showed clearly distinguished ODT peaks in the thermograms on cooling and heating at all temperature ramp rates, though they were substantially weaker than those observed from LAM samples, as shown for IL-14 in Figure 4B. The thermal signature of the ODT for BCC samples was only observed on heating and only after annealing the sample at temperatures below the T_{ODT} for a minimum of 30 min. The signature was so weak that it was almost outside the resolution of the DSC instrument and could only be reliably distinguished from baseline noise at high heating rates of 20°C/min, as shown for IL-15 in Figure 4C. Surprisingly, the temperature difference between the order-to-disorder transition temperature observed on heating (T_m) and disorder-to-order transition temperature observed on cooling (T_c) for the LAM and HEX forming samples was small, less than 5°C even at the relatively fast temperature ramp rate of

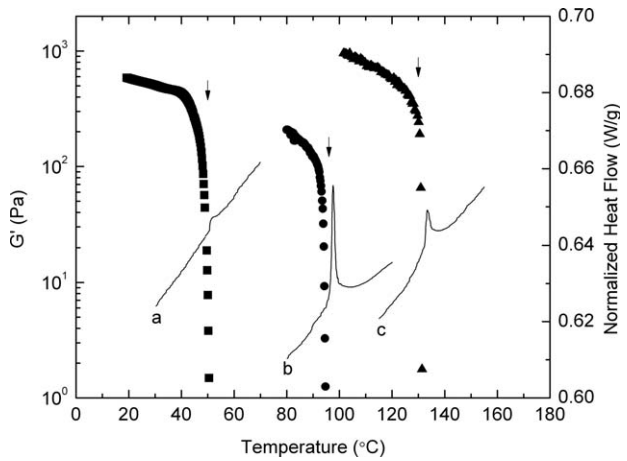

Figure 2. Determination of T_{ODT}.

Isochronal (0.1 rad/s) dynamic shear storage modulus, G', (filled symbols) and DSC thermograms (lines) obtained from IL-1 (curve b, filled circles), IL-14 (curve c, filled triangles), and IL-15 (curve a, filled squares) while heating at 0.1 (DMS) and 20°C/min (DSC). The DSC thermogram of IL-15 (curve a) was obtained after a 1-h isothermal annealing step at 40°C. The temperature at which a precipitous drop in G' is observed is regarded as the T_{ODT} and are marked with arrows. For clear presentation, DMS data for IL-15 (filled squares) and DSC data for IL-14 (curve c) have been shifted vertically by the factors of 10^{-2} and −0.6 W/g, respectively.

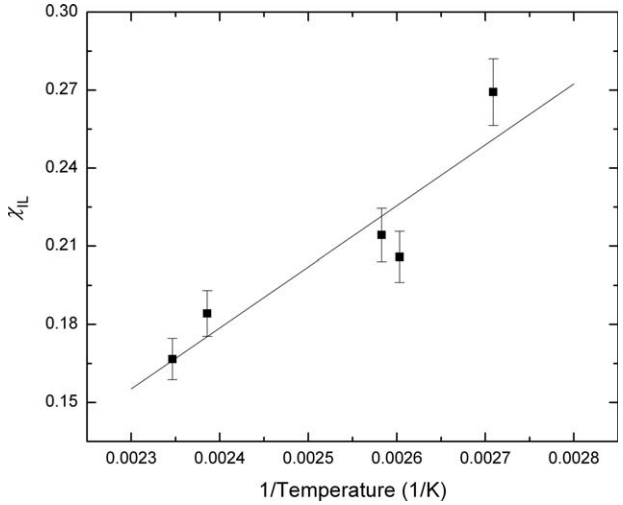

Figure 3. $\chi(T)$ for symmetric diblock copolymers.

The values of χ_{IL} were calculated based on the mean-field order-disorder criterion, $(\chi N)_{ODT}=10.5$ and the T_{ODT}'s of IL-1, 2, 3, 7, and 10 determined using DMS.

20°C/min, and became negligible as the heating and cooling rates were decreased. The HEX samples (IL-13, 14, and 5) produced slightly greater temperature differences between T_m and T_c, approximately 2–5°C at 20°C/min compared to 1–2°C for LAM at the same heating/cooling rate.

The nature of the ODT was also probed with SAXS experiments. Use of the synchrotron x-ray source enabled rapid data acquisition (ca. 5 s per frame) while changing the temperature at the same rates as was done with the DSC (see Figure 4). Selected SAXS patterns, collected while cooling and heating through the ODT of IL-1 at 10°C/min temperatures, are shown in Figure 5. Ordering and disordering occurs within the 1°C resolution of these experiments consistent with the DSC results. These results show that nucleation and growth of the LAM-forming samples is remarkably fast, consistent with our conclusion that the heat of the DIS-LAM transition recorded by DSC (see below) reflects an equilibrium value. Similar results were obtained on cooling and heating IL-14 (Figure 6), leading to the same assessment regarding the DIS-HEX transition.

The behavior of the sphere-forming specimens contrasts sharply with that documented with the LAM and HEX based materials, as illustrated in Figure 7 for IL-15. Cooling at 20°C/min from 100°C ($T_{ODT}+50$°C) to 0°C ($T_{ODT}-50$°C), fails to induce ordering, resulting in a SAXS pattern that contains a broad principal peak at $q^* \approx 0.065$ Å^{-1} and a weak bump at $q \approx 0.16$ Å^{-1}. We attribute these features to a liquid-like arrangement of spherical (micelle-like) aggregates.[26–29] As shown in a previous publication, annealing IL-15 for 30 min at 40°C following cooling from the disordered state leads to the development of BCC crystalline order (see Figure 1b).[30] These results are consistent with the DSC data found in Figure 4C.

Values for ΔH_{ODT}, the latent enthalpy of transition, were calculated from the DSC thermograms by integration of the endothermic (heating) and exothermic (cooling) peaks associated with the ODT. Latent enthalpies of the order-to-disorder transition, ΔH_m, and the disorder-to-order transition, ΔH_c, are listed in Table 3. For all the LAM-forming specimens, ΔH_m (0.31–0.36 J/g) was independent of the thermal history (i.e., cooling/heating rate and annealing time), and

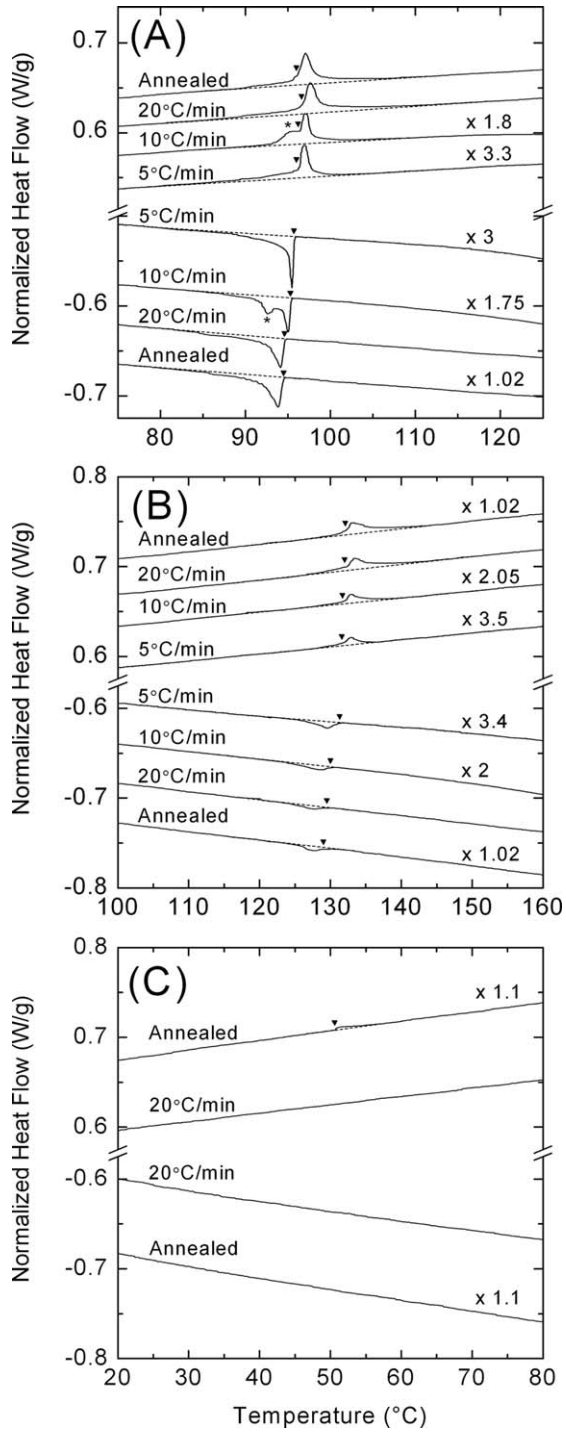

Figure 4. Differential scanning calorimetry measurements.

DSC thermograms obtained on cooling (below vertical axis break) and heating (above vertical axis break) at various temperature ramp rates obtained from (A) LAM forming IL-1, (B) HEX forming IL-14, and (C) BCC forming IL-15. Curves labeled "Annealed" were cooled and heated at 20°C/min with an additional 1-h annealing step (performed at 70, 110, and 40°C for samples IL-1, IL-14, and IL-15, respectively) between the initial cooling and final heating steps shown. Onset temperatures are marked with triangles and the dotted lines indicate baselines used in calculations of ΔH_{ODT}. Curves have been scaled by the factors indicated to allow the data for different temperature ramp rates to be clearly presented on a single set of axes.

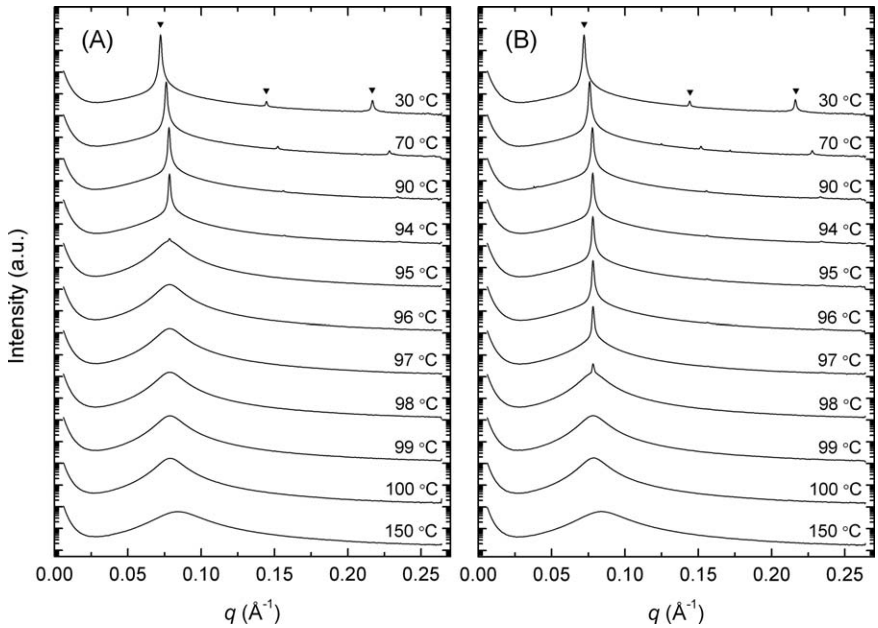

Figure 5. Temperature dependent SAXS for LAM forming sample IL-1.

Selected scattering patterns of LAM forming IL-1 obtained at the temperatures indicated *in situ* during dynamic temperature ramp SAXS experiments while (A) cooling and (B) heating at 10°C/min. Triangles above the 30°C curves mark the first several allowed Bragg reflections at relative peak positions of $q/q^* = 1, 2, 3$. Data from separate temperature ramps in which data were collected at 10°C and 1°C temperature intervals have been combined to clearly show the transition between order and disorder. The curves have been shifted vertically for clarity.

we believe this results represents an equilibrium value referred to as ΔH_{ODT}. However, the values of ΔH_c obtained for IL-1 (0.25–0.33 J/g) are actually slightly smaller than ΔH_m, where the quantitative difference decreases with decreasing cooling/heating rate. This result suggests some degree of (time-dependent) refinement of the ordered LAM phase (e.g., coarsening of the polydomain morphology) following ordering.

The cylinder-forming (HEX) specimens also displayed measureable ΔH_m and ΔH_c as listed in Table 3. Similar values of ΔH_m were extracted from IL-14 approximately independent of the thermal history. (There was a slight

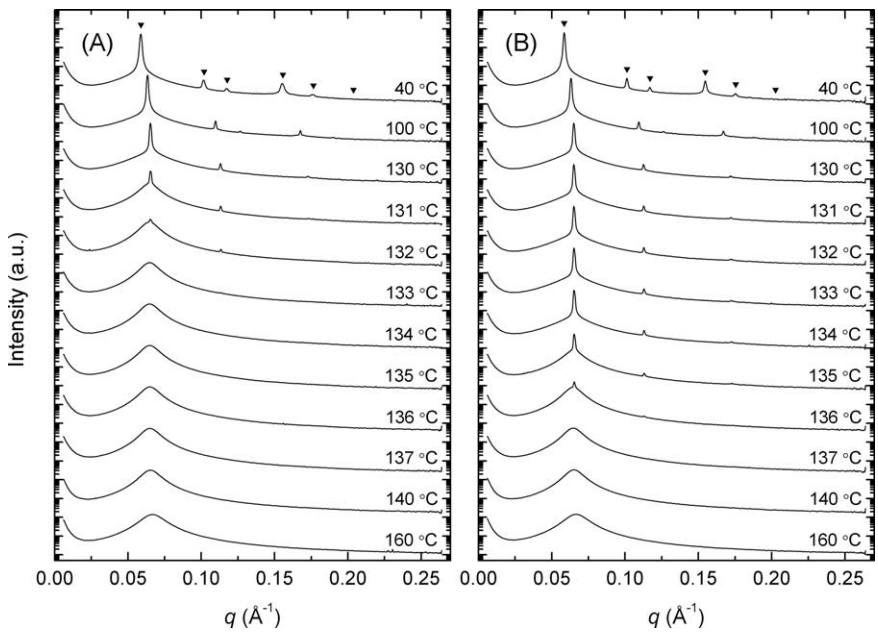

Figure 6. Temperature dependent SAXS for HEX forming sample IL-14.

Selected scattering patterns of HEX forming IL-14 obtained at the temperatures indicated *in situ* during dynamic temperature ramp SAXS experiments while (A) cooling and (B) heating at 10°C/min. Triangles above the 40°C curves mark the first several allowed Bragg reflections at relative peak positions of $q/q^* = \sqrt{1}, \sqrt{3}, \sqrt{4}, \sqrt{7}, \sqrt{9}, \sqrt{12}$. Data from separate temperature ramps in which data were collected at 10 and 1°C temperature intervals have been combined to clearly show the transition between order and disorder. The curves have been shifted vertically for clarity.

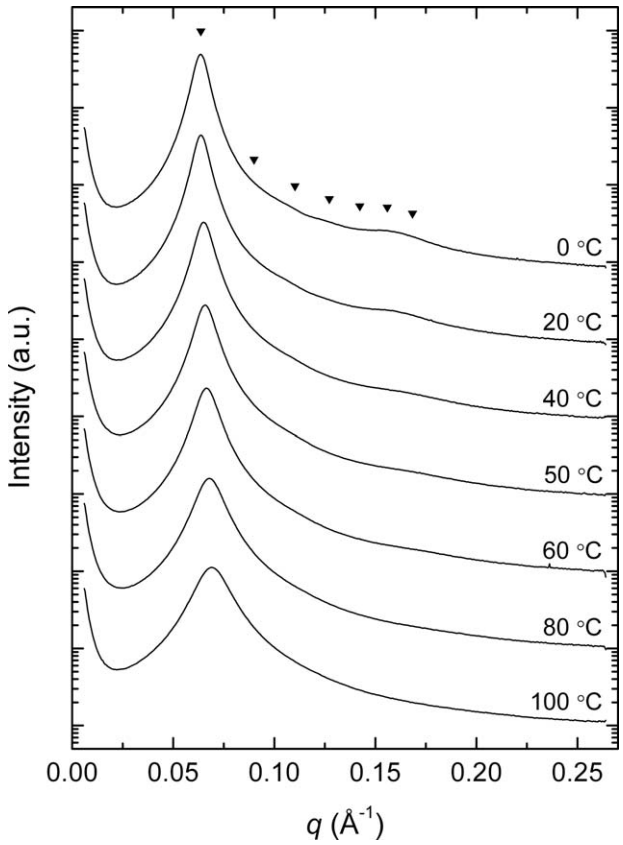

Figure 7. Temperature dependent SAXS for BCC forming sample IL-15.

Selected scattering patterns of BCC forming IL-15 obtained at the temperatures indicated *in situ* during dynamic temperature ramp SAXS experiments while cooling at 20°C/min. Triangles above the 0°C curve mark the first several allowed Bragg reflections at relative peak positions of $q/q^* = \sqrt{1}, \sqrt{2}, \sqrt{3}, \sqrt{4}, \sqrt{5}, \sqrt{6}, \sqrt{7}$. The curves have been shifted vertically for clarity.

dependence of ΔH_m with heating rate, i.e., larger values were obtained with faster experimental heating rates. We believe this minor difference can be attributed to systematic error associated with the limits of resolution of the DSC instrument). However, the magnitude of ΔH_c for IL-14 is two to five times smaller than ΔH_m in sharp contrast to the behavior of LAM-forming IL-1.

The BCC forming IL-15 also produced a (barely) measureable ΔH_m, but only at the fastest heating rate (20°C/min) and after annealing for at least 30 min, that is, the time required to transform the supercooled melt into a polycrystalline BCC material.[30] The measured value of ΔH_m was not sensitive to the annealing times longer than 30 min. Although the absolute value of ΔH_m measured for IL-15 is subject to a large absolute error (ca.±50%), the difference in magnitude relative to IL-1 (LAM) and IL-14 (HEX) is very significant.

Interestingly, IL-1 displays a second thermal transition at temperatures below the primary peak (marked by stars in Figure 4A) in DSC traces recorded at intermediate temperature ramp rates. Similar results were obtained with other LAM-forming samples (IL-2 and IL-3; not shown), but not with any of the HEX or BCC-forming materials. The size of this secondary peak appears to depend on the heating/cooling rate; expression of this feature at any heating rate is contingent on an intermediate cooling rate and is most pronounced at 10°C/min. Nevertheless, the overall integrated ΔH_{ODT} values are essentially independent of this feature. We do not know the origins of this behavior but note that there is no evidence of multiple structural features in the corresponding SAXS patterns (Figure 5).

Discussion

Our determination of $\chi_{IL}(T)$ is based on the assumption that the symmetric ($f_L \approx 1/2$) IL diblock copolymers conform with mean-field theory, that is, $(\chi N)_{ODT}=10.5$.[6,31] However, the absolute $(\chi N)_{ODT}$ values for the IL diblock copolymers must be somewhat higher than those determined based on mean-field theory due to local composition fluctuations, which are known to suppress T_{ODT}. Recent molecular simulations by Matsen and coworkers[32] indicate that $(\chi N)_{ODT} \approx 40$ for N values close to those considered in this work. Therefore, we expect the true value of χ_{IL} at a given temperature (e.g., one that also would account for the phase behavior of binary blends of PI and PLA homopolymers)[7] is substantially higher, perhaps four times as great, as what is determined by Eq. 1. Even so, the magnitude of the interaction parameter between PI and PLA was found to be quite large, greater than that for most hydrocarbon-based BCPs.[33,34] For example, with the common segment volume (110 Å^3) used in this work, polystyrene and PI are characterized at 140°C by $\chi_{SI}(140°C)=0.07$, compared to $\chi_{IL}(140°C)=0.18$, that is, approximately 2.5 times larger.[8] A larger χ parameter dictates a smaller molecular weight for polymers with experimentally accessible T_{ODT}s, leading to behavior near the ODT that is expected to be strongly influenced by large amplitude composition fluctuations in both the disordered and ordered states.

The IL diblock phase portrait constructed using Eq. 1 and Table 2 is presented in Figure 8. The overall features of the phase portrait are very similar to those of relatively weakly segregated systems, that is, for much larger N.[8,35,36] Compared to the ideal theoretical-phase portrait (assuming a conformationally symmetric system with perfect uniformity of chain length), the order-order phase boundaries are shifted toward slightly higher PLA compositions.[6,31] For a minority

Table 3. Calculated Enthalpies of Transition for Select IL Diblock Copolymers

Sample	IL-1 (LAM)	IL-14 (HEX)	IL-15 (BCC)*
Experiment	ΔH_m (ΔH_c), (J/g)	ΔH_m (ΔH_c), (J/g)	ΔH_m (ΔH_c), (J/g)
20°C/min w/ anneal	0.33† (0.25)‡	0.17§ (0.05)	0.02†† (–)
20°C/min	0.36 (0.25)‡	0.18 (0.03)	–
10°C/min	0.31 (0.29)‡	0.11 (0.07)‡	–
5°C/min	0.32 (0.33)‡	0.07 (0.08)	–
ΔH_{max}**	2.0	1.5	1.9

All experimental ΔH_m values were calculated from the final heating step of the experiments, whereas ΔH_c values, shown in parentheses, were calculated from the initial cooling step.
*Distinguishable peaks were only observed on heating and only in samples that were annealed before the final heating step.
†Annealed for 60 min at 70°C between initial cooling and final heating.
‡Average of values from multiple (2–4) experimental runs.
§Annealed for 60 min at 110°C between initial cooling and final heating.
††Annealed for 60 min at 40°C between initial cooling and final heating.
**Estimated from Eq. 2.

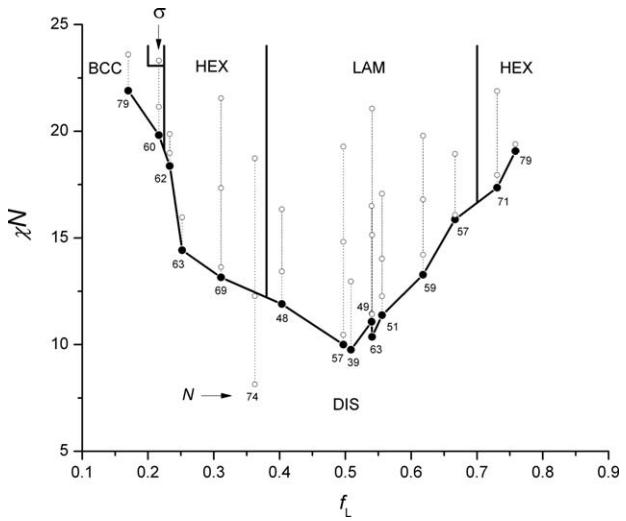

Figure 8. Experimental phase portrait for IL diblock copolymers.

The phase space points examined by SAXS are marked by white dots (○) and $(\chi N)_{ODT}$ identified by DMS based on the mean-field theory are marked by black dots (•). Below or near the $(\chi N)_{ODT}$ points, degrees of polymerization N are identified. Data points obtained from each sample are connected with dashed lines (···) and the interpolated phase boundaries are marked by solid lines (−).

of PLA, the HEX-LAM phase boundary is located at f_L, (HEX-LAM)=0.38±0.02 while at higher PLA content, f_L, (HEX-LAM)=0.70±0.02; in the strong segregation limit theory anticipates $f_A \cong 0.32$ and 0.68, respectively, for symmetric diblock copolymers.[31,37] Asymmetrically placed phase boundaries can be attributed to differences in block dispersities ($Đ=M_w/M_n>1$) and conformational asymmetry.[9–11,38] Although the dispersities of the PLA blocks are slightly higher than those of the PI counterparts (this can be deduced from the somewhat larger IL diblock copolymer dispersities compared to the PI values, see Table 1), we do not believe the modest shifts in the IL phase portrait can be attributed to these minor differences. Most likely, the locations of the phase boundaries reflect conformational asymmetry between PI and PLA: the ratio of statistical segment lengths, a, at a common reference volume at 140°C is $a_{PLA}/a_{PI} \approx 1.2$.[39,40] Several experimental studies of diblock copolymer-phase behavior have correlated a shift of the phase boundaries toward higher fractions of the blocks with the larger statistical segment length, which are consistent with the current findings and supported by self-consistent mean-field theory.[9]

Along with the classical ordered phases (LAM, HEX, BCC), the IL phase portrait contains the recently discovered Frank–Kasper σ-phase,[30] located at large values of χN between the BCC and HEX regions. This is consistent with the relative placement of the analogous phase in thermotropic dendritic liquid crystals.[41,42] The IL-16 (f_L=0.36 and N=74) is unusual in that an ordered HEX phase persists well-below the order-disorder phase boundary interpolated from neighboring samples (IL-14 and IL-11), and did not display any signature of an ODT by DMS and SAXS experiments up to 250°C (data are not shown). IL-16 has a PLA block, on average, just five lactide repeat units longer than IL-14 (f_L=0.31, N=69). These compounds were polymerized using the same polyisoprene precursor (I-4), yet resulted in very different $(\chi N)_{ODT}$ values. Surprisingly, IL-11 (f_L=0.40, N=48) showed $(\chi N)_{ODT}$=11.9, seemingly consistent with the overall ODT behavior exhibited by the complete set of IL diblock copolymers. We do not understand the origins of this anomaly. However, it may be another consequence of fluctuation effects, which introduce an additional N dependence to $(\chi N)_{ODT}$.[6,7]

The ODT must be accompanied by thermal effects that, in principle, should be amenable to characterization using calorimetric techniques. However, due a miniscule latent heat of transition ($\Delta H_{ODT} \sim \chi \sim N^{-1}$), such techniques have been of limited use with BCPs, even those with moderately low molecular weight. Although relatively rare, there have been several reports identifying the ODT by DSC.[13–15,17–19] Nevertheless, we are unaware of any systematic studies of such thermal features, that is, measurements of ΔH_{ODT} over a wide range of compositions covering three distinct morphologies as reported in this work.

A striking feature of Figures 4A, B is the almost negligible differences between T_m and T_c for the LAM and HEX forming specimens; $T_m - T_c \approx 0$ when the heating/cooling rate was lowered from 20 to 5°C/min. We believe this lack of hysteresis is a manifestation of composition fluctuations, and the resulting weakly first-order character of the associated phase transitions. Strong first-order phase transitions generally are governed by substantial free-energy barriers to nucleation leading to significant supercooling (superheating) as well-documented with water and other simple compounds during condensation (evaporation) and crystallization (melting).[43]

Another feature that implicates composition fluctuations is the magnitude and strong composition (i.e., ordered-state symmetry) dependence of ΔH_{ODT}, ranging from 0.36 J/g for IL-1 (LAM) to 0.02 J/g for IL-15 (BCC; see Table 3). These ΔH_{ODT} values are very small, several orders of magnitude lower than those associated with the crystallization of polymer chains; for example, the heat of fusion for PLA is 93 J/g.[44] In an effort to gain a better appreciation for the magnitude of these ΔH_{ODT} values, we consider two simples models, illustrated schematically for the DIS-LAM transition in Figure 9.

The maximum possible change in enthalpy for the ODT can be estimated as

$$\Delta H_{max} = \frac{RT_{ODT} f_L (1-f_L)\chi_{ODT} N}{M_n} - \frac{\Sigma \gamma_{IL}}{\rho} \qquad (2)$$

The first term on the right-hand side of Eq. 2 accounts for the difference in enthalpy between homogeneously mixed and completely separated (i.e., strongly segregated) PI and PLA segments, where R is the gas constant.[16] The second term deals with contact between segments at domain interfaces, where $\gamma_{IL} \approx (kT/a^2)\sqrt{\chi/6}$ is the interfacial tension[45] (k is Boltzmann's constant and a is the statistical segment length)[3] and Σ is the interfacial area per unit volume; for example, $\Sigma_{LAM}=2/D=q^*/\pi$ for the LAM morphology. Assuming $a \approx 0.63$ nm (the average of a_{PI} and a_{PLA} using a common 110 Å^3 segment reference volume), a density of 1 g/cm^3, and taking q^* from the SAXS results, yields estimated average values of ΔH_{max} for the LAM (2.0 J/g), HEX (1.5 J/g), and BCC (1.9 J/g) forming compounds (Table 3). These estimates are much larger than the experimentally determined heats of transition.

Alternatively, we can imagine that the transition from disorder to order involves almost no change in the local

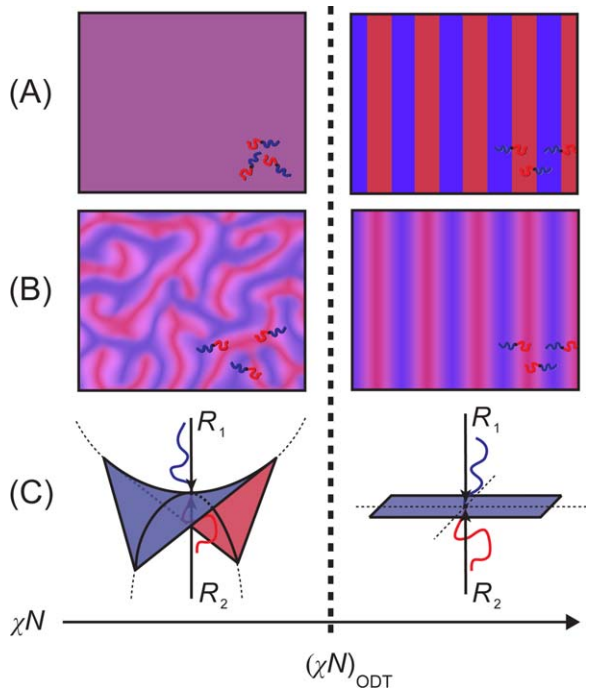

Figure 9. Schematic illustrations of order and disorder in LAM forming diblock copolymers.

(A) Formation of a LAM phase with pure domains and sharp interfaces from a homogeneous disordered phase resulting in the maximum possible enthalpy of transition, as estimated in Eq. 2. (B) Formation of a LAM phase from a fluctuating disordered phase. (C) Illustration of the curvature of the interface separating the domains for the situation depicted in (B) in which $R_1=-R_2 \approx R_g$ in the disordered state and $R_1=R_2 \approx \infty$ in the LAM phase. [Color figure can be viewed in the online issue, which is available at wileyonlinelibrary.com]

composition profile (i.e., the first term in Eq. 2 disappears) as depicted in Figure 9B. In this limit, a symmetric fluctuating bicontinuous disordered phase features domains with finite concentrations of PI and PLA divided by hyperbolic interfaces characterized by zero mean curvature ($H=[c_1+c_2]/2=0$, where $c_1=1/R_1$ and $c_2=1/R_2$), negative Gauss curvature ($K=c_1c_2<0$) and no spontaneous curvature ($c_o=0$).[46,47] Virtually, complete loss of higher-order diffraction, for example, extinction of $I(3q^*)$, as T approaches T_{ODT} (Figure 5) suggests that the LAM composition profile at the transition is essentially sinusoidal. Transition to a lamellar morphology produces flat interfaces with $H=0$, $K=0$, and $c_o=0$. Assuming there is no change in the local (instantaneous) composition profile, the heat of transition will reflect only the change in the topology of the interface separating the domains

$$\Delta H_{fluc}=\frac{\gamma_{AB}}{\rho}(\Sigma_{DIS}-\Sigma_{LAM}) \tag{3}$$

where Σ_{DIS} is the interfacial area per unit volume of the disordered phase. The disordered fluctuating state for LAM-forming diblock copolymers ($f_L=1/2$) is believed to be bicontinuous, similar to the structure observed during the late stages of spinodal decomposition,[48] hence $\Sigma_{DIS} \approx 0.5q^*$.[46] Setting $q^* = 0.078$ Å^{-1} (Figure 5) yields $\Delta H_{fluc} \approx 0.37$ J/g. This result is remarkably consistent with the value measured for IL-1 (Table 3). Although both estimates of ΔH_{ODT} (Eqs. 2 and 3) are relatively crude constructions (most seriously due to the mean-field assumption implicit in calculating χ), they lead us to favor the interpretation represented by Figures 9B, C, that is, a weakly first-order pattern transition that exchanges interfacial area for configurational entropy.

The SAXS data collected during temperature ramp experiments through the ODT further support our speculation that the ODT for LAM samples occurs with almost no change in the local composition profile. The total integrated scattering intensity (i.e., the total scattering power of a sample) known as the Porod invariant, Q, can be obtained by integrating the scattered intensity, $I(q)$, over all of reciprocal space. For an isotropic sample,[49]

$$Q=\frac{1}{2\pi^2}\int_0^\infty q^2 I(q)dq \tag{4}$$

The invariant reflects the extent of scattering length density inhomogeneity in a sample, which in the case of BCPs is directly linked to the local composition profile. For an ideal two-phase system consisting of regions of constant but differing scattering length densities separated by sharp boundaries (e.g., the LAM model in Figure 9A), the invariant calculated by Eq. 4 (with $I(q)$ in absolute intensity) reduces to

$$Q_{ideal}=(\Delta\rho)^2\phi_1\phi_2 \tag{5}$$

where ϕ_1 and ϕ_2 are the volume fractions of the two phases, and $\Delta\rho$ is the difference in scattering length density between the two regions. Q_{ideal} does not depend on how the two regions are arranged, hence the term invariant. SAXS data reported here were acquired on a relative intensity scale, hence the absolute magnitude of the invariant, and the associated composition profile, cannot be determined. The temperature dependence of the relative invariant, Q_{rel}, was calculated by integrating the background corrected intensity over $0.02 \le q \le 0.26$ Å^{-1}; this q range captures the entire measureable intensity in excess of the background scattering as illustrated in inset (b) of Figure 10 for IL-1. The temperature dependence of Q_{rel} determined for IL-1 while heating and cooling at 10°C/min is shown in Figure 10. Q_{rel} decreases approximately linearly with increasing temperature consistent with a graduate reduction in the degree of segregation between the PI and PLA blocks. Most significantly, Q_{rel} changes by less than 2% at the ODT consistent with little if any change in the local composition profile at the LAM-DIS transition in agreement with the case depicted in Figure 9B.

Remarkably, the LAM-DIS transition is accompanied by almost no change in $q^*(T)$ (Figure 11A), consistent with earlier studies based on higher molecular weight symmetric diblock copolymers.[21,47] As shown in the inset to Figure 11A q^* jumps by just 0.2% (i.e.,<0.02 nm) at the ODT. Nevertheless, individual chains are stretched considerably beyond the theoretical mean-field values at the ODT;[6] for IL-1 the periodic spacing, $D^* = 2\pi/q^* = 8$ nm (Figure 5), is more than 50% greater than $D_{MF}^* = (2\pi/1.95)R_g = 5.1$ nm, where $R_g=a(N/6)^{1/2}$. Apparently, loss of negative Gauss curvature does not influence local molecular packing constraints reinforcing the notion that the LAM-DIS transition rearranges the global interfacial curvature without significantly affecting the local composition density profile, H or c_o. These results leave open the possibility that $\Delta q^* \to 0$ at the ODT under precisely symmetric conditions (i.e., an AB

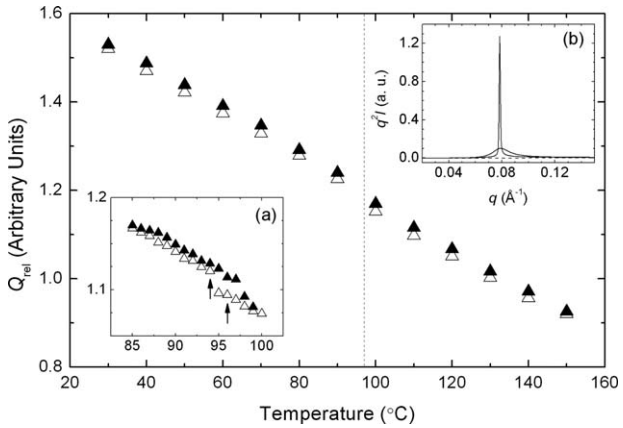

Figure 10. SAXS invariant near the ODT for sample IL-1.

Temperature dependence of the relative SAXS invariant, Q_{rel}, for LAM forming IL-1 calculated from temperature ramp SAXS experiments conducted at 10°C/min on heating (filled symbols) and cooling (open symbols). The vertical dotted line indicates the location of the ODT. Inset (a) shows data collected over a narrower temperature range in the vicinity of T_{ODT} on heating (filled symbols) and cooling (open symbols) at 10°C/min. Inset (b) shows SAXS patterns collected on cooling corresponding to the data points indicated by arrows in inset (a) at 96°C (DIS, broad peak) and 94°C (LAM, sharp peak) displayed as q^2I (related to the integrand of Eq. 4) as a function of q. The empty capillary data, which is subtracted from the experimental data prior to calculation of Q_{rel}, is shown as a dashed curve.

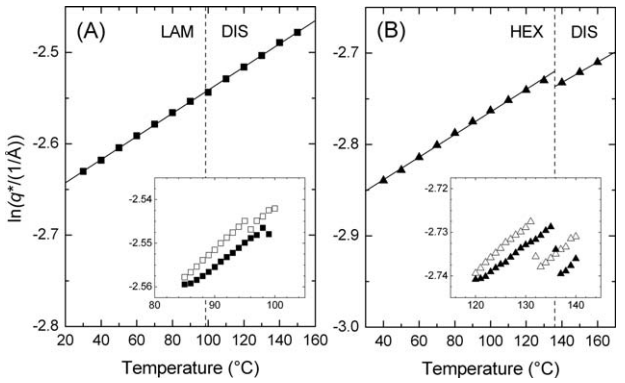

Figure 11. Temperature dependence of q^* near T_{ODT}.

(A) LAM forming IL-1 and (B) HEX forming IL-14 extracted from temperature ramp SAXS experiments conducted at 10°C/min on heating. Solid lines are linear fits to the data and dashed vertical lines indicate the locations of the ODTs. Insets show data collected over a narrower temperature range in the vicinity of T_{ODT} on heating (filled symbols) and cooling (open symbols) at 10°C/min.

diblock copolymer with $f_A=1/2$, $Đ=1$ and $a_A/a_B=1$); note that the small diffraction peaks at $2q^*$ in Figure 5 demonstrate that IL-1 is slightly off symmetry.

Taken together, the SAXS, DMS, and DSC results demonstrate that symmetric diblock copolymers belong to the Brazovskii universality class of fluctuation-induced weakly first-order phase transitions even in the limit of very low N. Reducing the composition to $f_L=0.31$ (sample IL-14) changes the nature of the ODT. As shown in Figure 11B, q^* exhibits a small (ca. 1%) but distinct discontinuity at the DIS-HEX transition, which we associate with qualitative differences in the interfacial properties of the ordered ($H\neq0$, $K=0$ and $c_o\neq0$ for a cylindrical morphology) and fluctuating disordered states. A modestly asymmetric composition likely narrows the difference between the fluctuating disordered and ordered morphologies, driving down ΔH_{ODT}, relative to the symmetric ($f_L=1/2$) case (Table 3).

More dramatic thermodynamic and structural differences were obtained with $f_L=0.22$, where the ordered-state morphology is spherical ($H\neq0$, $K=0$ and $c_o\neq0$). In this limit, ΔH_{ODT} nearly disappears (Table 3) and the rate of ordering drops by orders of magnitude, that is, 30 min at 40°C (BCC) and more than a day at 25°C (σ-phase).[30] We believe these changes can be explained based on the structure of the disordered state as depicted in Figure 12. As the temperature approaches T_{ODT} asymmetric composition fluctuations will be manifested as discreet micelles as anticipated theoretically by Semenov[50] in the limit $f \rightarrow 0$. The presence of micelles in the disordered state has been demonstrated using a variety of experimental techniques including DMS, SAXS, small-angle neutron scattering, transmissions electron microscopy, and x-ray photon correlation spectroscopy.[26,27,51–53] Because the disordered and solid (crystalline) phases are characterized by the same domain morphology, no change in interfacial topology occurs during ordering, that is, $\Sigma_{DIS} \cong \Sigma_{BCC}$ with essentially constant $H\neq0$, and $c_o\neq0$ and $K=0$. We believe this explains the drastic reduction in ΔH_{ODT}.

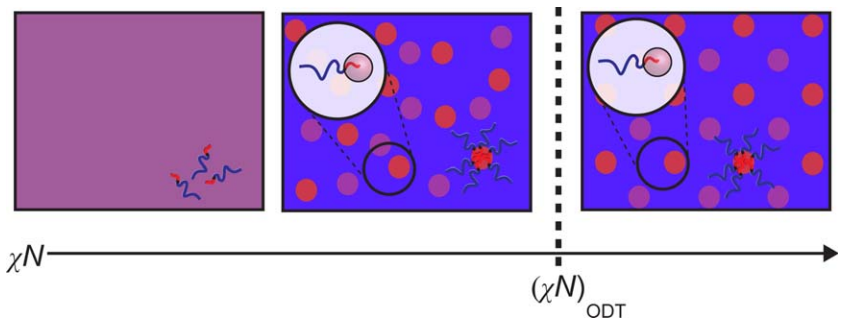

Figure 12. Schematic illustration of order and disorder in sphere forming diblock copolymers.

At low χN (high temperature for a fixed N sample) a homogeneous and isotropic disordered phase exists (left panel). As χN increases (temperature decreases) to approach the ODT, composition fluctuations result in a disordered phases that contains micelles (middle panel). At the ODT, the micelles order on a BCC lattice with minimal change to the interface between the blue and red domains (right panel). [Color figure can be viewed in the online issue, which is available at wileyonlinelibrary.com]

Assuming the small bump that appears at high q in the SAXS patterns in Figure 7 corresponds to the first maxima in the spherical form factor ($qR=5.76$), we estimate a micelle core radius of $R=3.5$ nm. Combined with the BCC lattice spacing of $a=13.7$ nm extracted from Figure 1b yields a volume fraction of spheres at the ODT of $f_{\text{spheres}} \approx 0.14$. This value is less than f_L suggesting that a portion of the PLA blocks remain dissolved in the PI matrix. This may help to explain the existence of the σ-phase by analogy with the multiplicity of ordered spherical states predicted by Semenov[50] near the ODT in the asymmetric limit $f \rightarrow 0$.

Conclusions

This report describes the thermodynamic behavior of a series of model high χ and low N poly(1,4-isoprene-*b*-DL-lactide) BCPs near the ODT. The measured structural and thermal characteristics of the ODT, particularly the magnitude of ΔH_{ODT} and the strong dependence of ΔH_{ODT} on ordered-phase morphology, provide direct evidence that supports an interpretation of the ODT in BCPs as a weakly first-order phase transition dominated by the effects of local composition fluctuations. Weakly first-order, fluctuation-driven, phase transitions are known to occur in many physical systems,[54] ranging from technologically important materials (e.g., isotropic-nematic[55] and nematic-smectic[56,57] transitions in liquid crystals, certain types of superconductors,[58] and magnetic alloys[59]) to more exotic forms of condensed matter (e.g., Bose–Einstein condensation of ultracold atoms[60]). Multiblock polymers offer convenient experimental systems for studying this fascinating class of phase transitions while providing access to industrially relevant nanostructured materials. An added dividend of the work reported here is direct contact with computer simulations, potentially exact analogues of our experimental system, made feasible by the reduced molecular size.[32,61]

Acknowledgments

This work was supported by the National Science Foundation under award 0704192. Portions of this work were performed at the DuPont-Northwestern-Dow Collaborative Access Team (DND-CAT) located at Sector 5 of the Advanced Photon Source (APS). DND-CAT is supported by E.I. DuPont de Nemours & Co., The Dow Chemical Company, and Northwestern University. Use of the APS, an Office of Science User Facility operated for the U.S. Department of Energy (DOE) Office of Science by Argonne National Laboratory, was supported by the U.S. DOE under Contract No. DE-AC02-06CH11357. Parts of this work were carried out in the University of Minnesota, College of Science and Engineering Characterization Facility, which receives partial support from NSF through the National Nanotechnology Infrastructure Network program.

Literature Cited

1. Bates FS, Hillmyer MA, Lodge TP, Bates CM, Delaney KT, Fredrickson GH. Multiblock polymers: panacea or pandora's Box? *Science*. 2012;336(6080):434–440.
2. Hamley IW. The Physics of Block Copolymers. Oxford: Oxford Univ. Press, 1998.
3. Bates FS, Fredrickson GH. Block copolymers-designer soft materials. *Phys Today*. 1999;52(2):32–38.
4. Lodge TP. Block copolymers: past successes and future challenges. *Macromol Chem Phys*. 2003;204(2):265–273.
5. Stoykovich MP, Nealey PF. Block copolymers and conventional lithography. *Mater Today*. 2006;9(9):20–29.
6. Leibler L. Theory of microphase separation in block copolymers. *Macromolecules*. 1980;13(6):1602–1617.
7. Fredrickson GH, Helfand E. Fluctuation effects in the theory of microphase separation in block copolymers. *J Chem Phys*. 1987;87(1):697–705.
8. Khandpur AK, Förster S, Bates FS, Hamley IW, Ryan AJ, Bras W, Almdal K, Mortensen K. Polyisoprene-polystyrene diblock copolymer phase diagram near the order-disorder transition. *Macromolecules*. 1995;28(26):8796–8806.
9. Matsen MW, Bates FS. Conformationally asymmetric block copolymers. *J Poly Sci B: Poly Phys Ed*. 1997;35(6):945–952.
10. Lynd NA, Hillmyer MA. Influence of polydispersity on the self-assembly of diblock copolymers. *Macromolecules*. 2005;38(21):8803–8810.
11. Matsen MW. Polydispersity-induced macrophase separation in diblock copolymer melts. *Phys Rev Lett*. 2007;99(14):148304.
12. Brazovskii SA. Phase transition of an isotropic system to a nonuniform state. *Soviet Phys JETP*. 1975;41:85–89.
13. Stühn B. The relation between the microphase separation transition and the glass transition in diblock copolymers. *J Poly Sci B: Poly Phys Ed*. 1992;30(9):1013–1019.
14. Kasten H, Stühn B. Density discontinuity at the microphase separation transition of a symmetric diblock copolymer. *Macromolecules*. 1995;28(13):4777–4778.
15. Voronov VP, Buleiko VM, Podneks VE, Hamley IW, Fairclough JPA, Ryan AJ, Mai SM, Liao BX, Booth C. A High-resolution calorimetry study of the order−disorder transition in a diblock copolymer melt. *Macromolecules*. 1997;30(21):6674–6676.
16. Hajduk DA, Gruner SM, Erramilli S, Register RA, Fetters LJ. High-pressure effects on the order−disorder transition in block copolymer melts. *Macromolecules*. 1996;29(5):1473–1481.
17. Floudas G, Hadjichristidis N, Stamm M, Likhtman AE, Semenov AN. Microphase separation in block copolymer/homopolymer blends: theory and experiment. *J Chem Phys*. 1997;106(8):3318–3328.
18. Hillmyer MA, Bates FS. Influence of crystallinity on the morphology of poly(ethylene oxide) containing block copolymers. *Macromol Symp*. 1997;117:121–130.
19. Kim JK, Lee HH, Gu Q-J, Chang T, Jeong YH. Determination of order−order and order−disorder transition temperatures of sis block copolymers by differential scanning calorimetry and rheology. *Macromolecules*. 1998;31(12):4045–4048.
20. Rosedale JH, Bates FS. Rheology of ordered and disordered symmetric poly(ethylenepropylene)-poly(ethylethylene) diblock copolymers. *Macromolecules*. 1990;23(8):2329–2338.
21. Rosedale JH, Bates FS, Almdal K, Mortensen K, Wignall GD. Order and disorder in symmetric diblock copolymer melts. *Macromolecules*. 1995;28(5):1429–1443.
22. Brandrup J, Immergut EH. Polymer Handbook, 3rd ed. New York: Wiley, 1989.
23. Schmidt SC, Hillmyer MA. Morphological behavior of model poly (ethylene-alt-propylene)-b-polylactide diblock copolymers. *J Polym Sci Part B: Polym Phys*. 2002;40(20):2364–2376.
24. Schmidt SC, Hillmyer MA. Synthesis and characterization of model polyisoprene−polylactide diblock copolymers. *Macromolecules*. 1999;32(15):4794–4801.
25. Fetters LJ, Lohse DJ, Richter D, Witten TA, Zirkel A. Connection between Polymer Molecular Weight, Density, Chain Dimensions, and Melt Viscoelastic Properties. *Macromolecules*. 1994;27(17):4639–4647.
26. Schwab M, Stühn B. Thermotropic transition from a state of liquid order to a macrolattice in asymmetric diblock copolymers. *Phys Rev Lett*. 1996;76:924–927.
27. Wang X, Dormidontova EE, Lodge TP. The order−disorder transition and the disordered micelle regime for poly(ethyleneпropylene-b-dimethylsiloxane) spheres. *Macromolecules*. 2002;35(26):9687–9697.
28. Abuzaina FM, Patel AJ, Mochrie S, Narayanan S, Sandy A, Garetz BA, Balsara NP. Structure and phase behavior of block copolymer melts near the sphere−cylinder boundary. *Macromolecules*. 2005;38(16):7090–7097.
29. Han CD, Vaidya NY, Kim D, Shin G, Yamaguchi D, Hashimoto T. Lattice disordering/ordering and demicellization/micellization transitions in highly asymmetric polystyrene-block-polyisoprene copolymers. *Macromolecules*. 2000;33(10):3767–3780.

30. Lee S, Bluemle MJ, Bates FS. Discovery of a Frank-Kasper σ-phase in sphere-forming block copolymer melts. *Science*. 2010;330(6002): 349–353.
31. Cochran EW, Garcia-Cervera CJ, Fredrickson GH. Stability of the gyroid phase in diblock copolymers at strong segregation. *Macromolecules*. 2006;39(7):2449–2451.
32. Vassiliev ON, Matsen MW. Fluctuation effects in block copolymer melts. *J Chem Phys*. 2003;118(16):7700–7713.
33. Cochran EW, Bates FS. Thermodynamic behavior of poly(cyclohexylethylene) in polyolefin diblock copolymers. *Macromolecules*. 2002;35(19):7368–7374.
34. Barton AFM. CRC Handbook of Polymer-Liquid Interaction Parameters and Solubility Parameters. Boston, MA: CRC Press, 1990.
35. Schulz MF, Khandpur AK, Bates FS, Almdal K, Mortensen K, Hajduk DA, Gruner SM. Phase behavior of polystyrene−poly(2-vinylpyridine) diblock copolymers. *Macromolecules*. 1996;29(8):2857–2867.
36. Mai S-M, Fairclough JPA, Terrill NJ, Turner SC, Hamley IW, Matsen MW, Ryan AJ, Booth C. Microphase separation in poly(oxyethylene)−poly(oxybutylene) diblock copolymers. *Macromolecules*. 1998;31(23):8110–8116.
37. Matsen MW, Bates FS. Unifying weak- and strong-segregation block copolymer theories. *Macromolecules*. 1996;29(4):1091–1098.
38. Lynd NA, Hillmyer MA. Effects of polydispersity on the order−disorder transition in block copolymer melts. *Macromolecules*. 2007;40(22):8050–8055.
39. Shefelbine TA, Vigild ME, Matsen MW, Hajduk DA, Hillmyer MA, Cussler EL, Bates FS. Core−shell gyroid morphology in a poly(isoprene-block-styrene-block-dimethylsiloxane) triblock copolymer. *J Am Chem Soc*. 1999;121(37):8457–8465.
40. Anderson KS, Hillmyer MA. Melt chain dimensions of polylactide. *Macromolecules*. 2004;37(5):1857–1862.
41. Ungar G, Liu Y, Zeng X, Percec V, Cho W-D. Giant supramolecular liquid crystal lattice. *Science*. 2003;299(5610):1208–1211.
42. Ungar G, Zeng X. Frank–Kasper, quasicrystalline and related phases in liquid crystals. *Soft Matter*. 2005;1:95–106.
43. Chaikin PM, Lubensky TC. Principles of Condensed Matter Physics. Cambridge: Cambridge Univ. Press, 1995.
44. Fischer EW, Sterzel HJ, Wegner G. Investigation of the structure of solution grown crystals of lactide copolymers by means of chemical reactions. *Coll Polym Sci*. 1973;251(11):980–990.
45. Helfand E, Tagami Y. Theory of the interface between immiscible polymers. *J Polym Sci Part B: Polym Lett*. 1971;9(10):741–746.
46. Jinnai H, Koga T, Nishikawa Y, Hashimoto T, Hyde ST. Curvature determination of spinodal interface in a condensed matter system. *Phys Rev Lett*. 1997;78(11):2248–2251.
47. Bates FS, Rosedale JH, Fredrickson GH. Fluctuation effects in a symmetric diblock copolymer near the order-disorder transition. *J Chem Phys*. 1990;92(10):6255–6270.
48. Bates FS, Fredrickson GH. Block copolymer thermodynamics: theory and experiment. *Ann Rev Phys Chem*. 1990;41(1):525–557.
49. Porod G: Die Röntgenkleinwinkelstreuung von dichtgepackten kolloiden Systemen. *Kolloid Z*. 1951;124(2):83–114.
50. Semenov AN. Contribution to the theory of microphase layering in block-copolymer melts. *Soviet Phys JETP*. 1985;61:733–742.
51. Dormidontova EE, Lodge TP. The order−disorder transition and the disordered micelle regime in sphere-forming block copolymer melts. *Macromolecules*. 2001;34(26):9143–9155.
52. Wang J, Wang Z-G, Yang Y. Nature of disordered micelles in sphere-forming block copolymer melts. *Macromolecules*. 2005;38(5): 1979–1988.
53. Patel AJ, Narayanan S, Sandy A, Mochrie SGJ, Garetz BA, Watanabe H, Balsara NP. Relationship between structural and stress relaxation in a block-copolymer melt. *Phys Rev Lett*. 2006;96(25):257801.
54. Binder K. Theory of first-order phase transitions. *Rep Prog Phys*. 1987;50(7):783–859.
55. Van Roie B, Leys J, Denolf K, Glorieux C, Pitsi G, Thoen J. Weakly first-order character of the nematic-isotropic phase transition in liquid crystals. *Phys Rev E*. 2005;72(4):041702.
56. Martínez-Miranda LJ, Kortan AR, Birgeneau RJ. X-ray study of fluctuations near the nematic-smectic-a-smectic-c multicritical point. *Phys Rev Lett*. 1986;56(21):2264–2267.
57. Anisimov MA, Cladis PE, Gorodetskii EE, Huse DA, Podneks VE, Taratuta VG, Saarloos WV, Voronov VP. Experimental test of a fluctuation-induced first-order phase transition: the nematic–smectic-A transition. *Phys Rev A*. 1990;41(12):6749–6762.
58. Dalidovich D, Yang K. Fluctuation-driven first-order transition in pauli-limited d-wave superconductors. *Phys Rev Lett*. 2004;93(24): 247002.
59. Janoschek M, Garst M, Bauer A, Krautscheid P, Georgii R, Boni P, Pfleiderer C. Fluctuation-induced first-order phase transition in Dzyaloshinskii-Moriya helimagnets. arXiv.org e-Print archive. 2012; arXiv:1205.4780v1. http://arxiv.org/abs/arXiv:1205.4780v1 (Accessed September 15, 2012).
60. Gopalakrishnan S, Lev BL, Goldbart PM. Emergent crystallinity and frustration with Bose-Einstein condensates in multimode cavities. *Nat Phys*. 2009;5(11):845–850.
61. Beardsley T, Matsen M. Monte Carlo phase diagram for diblock copolymer melts. *Eur Phys J E: Soft Matter Biol Phys*. 2010;32(3): 255–264.

Manuscript received Sept. 29, 2012, and final revision received Jan. 7, 2013.